



MALAYSIAN JOURNAL OF BIOCHEMISTRY & MOLECULAR BIOLOGY

The Official Publication of The Malaysian Society For Biochemistry & Molecular Biology
(MSBMB)
<http://mjbmb.org>

INSIGHTS INTO THE DYNAMIC DOMAIN FLUCTUATIONS AND SIGNAL PROPAGATION OF ALLOSTERIC REGULATION IN PYRUVATE KINASE IN *Mycobacterium tuberculosis*

Pavan Gollapalli^{*1}, Aditya Rao SJ², Shivananda Kandagalla³, Sharath Belenahalli Shekarappa³, Manjunath Chavadi⁴, and Manjunatha Hanumanthappa^{*,3,5}

¹Central Research lab, K.S. Hegde Medical Academy, NITTE (Deemed to be University), Deralakatte, Mangaluru-575018, Karnataka, India.

²Plant Cell Biotechnology Department, CSIR-Central Food Technological Research Institute, Mysore-570020, Karnataka, India.

³Department of Biotechnology and Bioinformatics, Jnana Sahyadri, Kuvempu University, Shankaraghatta-577451, Karnataka, India

⁴Department of Biotechnology, Gulbarga University, Kalaburgi- 585106, Karnataka, India

⁵Department of Biochemistry, Jnana Bharathi Campus, Bangalore University, Bangalore, Karnataka, 560056, India

*Corresponding author: manjunathh@kuvempu.ac.in; gollapallipavan@nitte.edu.in

History

Received: 3rd December 2020

Accepted: 17th March 2021

Keywords:

MD simulation; Normal mode analysis; Principal Component Analysis; B-factors; Molecular docking

Abstract

The enzyme's structure-based function relationship suggested that pyruvate kinase regulation acts as a pivotal step in the energy management of *Mycobacterium tuberculosis* during infection. The present study aims to understand the network of interactions between the ligands Adenosine monophosphate (AMP) and Glucose-6-phosphate (G6P) during their allosteric regulation of pyruvate kinase (pyk) from *M. tuberculosis* with its imposed structural stability via dynamic domain fluctuations and signal propagation using molecular dynamics simulations studies. The results revealed that the molecular re-arrangement and associated conformational modifications after the smooth binding of AMP and G6P to pyruvate kinase result in reduced enzyme flexibility. Further, based on the signal propagation rate, the residues involved in the mediation of allosteric communication between the domains during fluctuation to regulate pyruvate kinase enzyme allostereism were predicted. The synergistic assistance of two allosteric binding sites for AMP and G6P in *M. tuberculosis* pyk monomer provides a piece of evidence for the existence of two physical allosteric pathways in the bacterium to regulate several metabolic processes.

INTRODUCTION

Global exploration on multi-drug resistance research survey among the Mycobacterial clinical isolates has revealed the elevated tuberculosis incidents in recent times [1]. The human hosts get infected inside the alveolar tissues of the lungs by inhaling the infectious aerosols. After infection, a long period of the quiescent state is established in the pathogen, during which the metabolic shift from aerobic to

an anaerobic state can be observed. This shift also affects the gene expression of the glycolytic pathway enzymes [2].

The details of bacterial metabolism and physiology during the infection process are limited. Thus, understanding the importance of nutrients in the hostile microenvironment becomes vital to access metabolic regulations adopted by the pathogen during growth and replication [3–8]. The genome sequence data helps in this regard by characterizing the pathways involved in the growth and replication of the pathogen and deciphers the variations in species-specific

enzymes [9]. The genome sequence of *M. tuberculosis* (Mtb) can thus provide an opportunity to spot the genes involved in glucose metabolism [10]. The differences in the biochemical properties of metabolic enzymes and their structural variations across different species can also be exploited to understand the infection mechanism and later can be used to identify drug targets specific to metabolic pathways.

The study of structural features in relation to functions is of prime importance to understand the effect of regulatory molecules on the allosteric nature of pyruvate kinase. Structurally, the bacterial pyruvate kinase comprises three distinct domains, viz, A, B, and C. The cleft between the A and B domain (lid domain) forms the active site location for substrate binding, while the C-domain harbours a canonical AMP allosteric site. The region between A and C domain provides an allosteric binding site for glucose-6-phosphate (G6P) [11-13]. Pyruvate kinase undergoes tight allosteric regulation, which allows the tetramerization through A and C domain interacting with adjacent monomer subunits leading to the formation of large A-A interface in A domain and small C-C interface in adjacent C domain between monomers [12, 14]. In *M. tuberculosis*, the pyruvate kinase requires disruption of C-C interface interactions between the AMP loop and C-terminal tail loop in addition to the formation of hydrogen bonds between adjacent C α 4 structures. This interplay between the AMP loop and the C-terminal tail loop facilitates the transition between tensed 'T' state and the relaxed 'R' state of the regulation of pyk [15-18]. The binding of effectors (G6P and AMP) or substrate (PEP) molecule to pyruvate kinase will manifest its allosteric behaviour [19]. Allosteric regulation serves as an important mechanism that controls multiple cellular processes like signal transduction, transcription and metabolism [8].

An alteration in protein conformation is mediated by allosteric effects with the contribution of entropy rather than protein structure. The conformational modification of the active site is associated with the allosteric effect that transmits signals throughout the protein [17]. Moreover, the allosteric mechanism and structural foundation to analyse the mode of transition leading to the formation of various conformations of pyruvate kinase due to flexible regions could provide an opportunity to design new strategies to target *M. tuberculosis* connected health problems. Accordingly, we have described the Molecular Dynamics (MD) of pyruvate kinase monomer in the absence and presence of allosteric effectors (AMP and G6P) using computational simulations. The investigation is based on the computational modelling of *M. tuberculosis* pyk protein for deciphering the structure-based physiological effect of binding of AMP and G6P at the allosteric site, which could be a potential target for future therapeutic research.

MATERIALS AND METHODS

Molecular Docking of Allosteric Activators

The comparative modelling was performed to obtain the 3D structure of the target pyruvate kinase protein using the MODELLER software suite [20] and validated as described in our earlier work [21]. For docking studies, the structures of phosphoenolpyruvate (CID: 1005: PEP), Glucose-6-phosphate (CID: 5958: G6P) and Adenosine monophosphate (CID: 6083: AMP) were retrieved from the PubChem database (<https://pubchem.ncbi.nlm.nih.gov/>) [22]. The selected 3D structures of the ligands were further optimized with ChemsSketch V.12.01 software [23].

Prior to the docking analysis, the prominent binding site of pyruvate kinase was predicted using AlloSite version 2.0 [24, 25]. Autodock tools was used for molecular docking to analyse the binding energies, and the docked complex was used for molecular dynamic simulations [26, 27]. Briefly, the Lamarckian genetic algorithm (LGA) implemented in AutoDock V.4.2 was employed in the study [28]. For the ligand molecules, all the torsions were allowed to rotate during docking. The grid box was set around the residues forming the active pocket [27, 29], and the Grid log file was generated using AutoGrid program and the pseudo-Solis and Wets methods were applied for energy minimization using default parameters to generate dock parameter file [30].

Molecular Dynamic (MD) Simulations

The MD simulation was carried out for the structure obtained from homology modelling of pyruvate kinase as native structure and for the docked complexes. The GROMACS (GROningen MAchine for Chemical Simulation) package version 4.5.5 [31] was used to conduct all the simulations, with the GROMACS force field 4301 parameter sets. The solvation of starting structures was attained in a dodecahedron box placed at a distance of 0.9 nm from the box boundary. A coupling time of 0.4 ps was used to couple the solute and the solvent separated to a temperature reservoir. The NPT equilibrium was achieved by maintaining the pressure isotropically at 1 bar through a coupling constant of 0.1 ps utilizing the Berendsen thermostat [32]. A Leapfrog algorithm was equated by integrating motions with a time step of 2 fm. The SHAKE algorithm [33] was used to constrain the covalent bond length between hydrogen and heavy atoms with a relative geometric tolerance of 0.0001. A steepest-descent minimization protocol was considered for equilibration [34].

Principal Component Analysis (PCA)

Principal components stand as a valuable tool for analyzing the conformational changes which are performed on Cartesian coordinates or dihedral analysis (dPCA). A typical MD trajectory which contains time-evaluated information

was used for principal component analysis to extract dominant modes in the motion of the molecular complex. This MD step is an order of 1 fm with the time ranging from one to ten nanoseconds (ns) for the simulation with a resulting trajectory of huge data that can be extracted accordingly. The concerted atomic displacements from the set of experimental structures will feature large conformational changes within the structure, which can be evaluated by principal component analysis [35], as the physiological functions of a protein depended on these motions. In the PCA, the input system possessing N atoms was constructed as a trajectory matrix by specifying each column with Cartesian coordinates for a given atom of each output time step. During PCA, the trajectory data generated by a long-time MD simulation were processed in diagonalization of 3N covariance matrices. MD-PCA was performed with the same thermostatic environment as in reference molecule simulation with a time step dependent ignoring overall rotation and translation [36].

Covariance Matrix

The final MD trajectories were used for the construction of covariance matrix. The degree of co-linearity of atomic motion was captured for each pair of the atoms to obtain a covariance matrix in the PCA. The subsequent diagonalization of the covariance matrix yields an eigenvector matrix and eigenvalues with a diagonal matrix. Eigenvectors describe the collective motions of the particles with values that indicate the corresponding atomic motions. The associated eigenvalues describe the sum of fluctuations by the collective individual atomic motions, which in total measures the modelling associated with eigenvectors [37].

Elastic Network Models to Study the Collective Dynamics of Pyruvate Kinase

The information on conformational dynamics of pyruvate kinase from *M. tuberculosis* was determined by using DynOmics web server (<http://dynamics.pitt.edu/>) [38]. The server evaluates molecular motions for reconstructing all atomic resolutions, mean-square fluctuations profile and comparison with B-factors, shape, dispersion and degree of collectivity of individual modes of motions and cross-correlation between residue fluctuations, IDD-based domain separations, PFSs derived from mode shape, residues acting as sensors and effectors or mediators of allosteric communication, based on signal propagation (hitting) rates

and key residues that potentially mediate allosteric communication [38].

RESULTS

Interaction of Enzyme with Allosteric Activators

The binding mode of the allosteric activators adenosine-5'-monophosphate (AMP) and glucose-6 phosphate (G6P) with the enzyme pyruvate kinase from *M. tuberculosis*, performed using Autodock 4.2 followed by visualization of the docked complexes by Discovery Studio software (Figure 1). Table 1 details the prominent binding sites predicted by AlloSite version 2.0. The predicted binding energy for the interactions of the target enzyme with G6P was -6.3 Kcal/mol indicating the strong binding energy of the activator; on the other hand, the binding energy of AMP was -7.6 Kcal/mol indicating the stronger binding towards pyk (Table 2). Docking analysis has revealed the involvement of arginine, leucine, asparagine, serine, threonine, valine, lysine, aspartic acid, glutamine, tryptophan, proline, histidine and phenylalanine as most prominent amino acid residues in forming the binding site signifying their role in determining the binding strength and reaction contribution in the formation of H-bonds (SI 3). The formation of hydrophobic interactions, Van der Waals forces, ionic bonds, charged interactions and H-bonds are contributed by the amino acid residues such as Pro, His, Gly and Glu. Global energy score, attractive or repulsive Van der Waals, and ACE and predicted binding energy were considered for the analysis of the binding strength of docked complexes, pyk-G6P and pyk-AMP, respectively (SI 4).

Molecular Dynamics of pyk Associated with Allosteric Regulation

Selection of Structures for MD Simulation

The folded structure of pyruvate kinase in *M. tuberculosis* consists of three conserved domains of which A-domain comprises of the residues from 1-70 and 168-336, the B-domain which forms the mobile lid comprises the residues from 71-167 and the C-domain that span the effector site, comprises of the residues from 337-472. The AMP binding loop comprises residues 451-458 and G6P binding loop with residues 345-349 (SI 1). For detailed comparison of the *M. tuberculosis* pyruvate kinase, the structure without ligand in the T-state and the docked complexes with G6P and AMP were considered for molecular dynamics simulation.

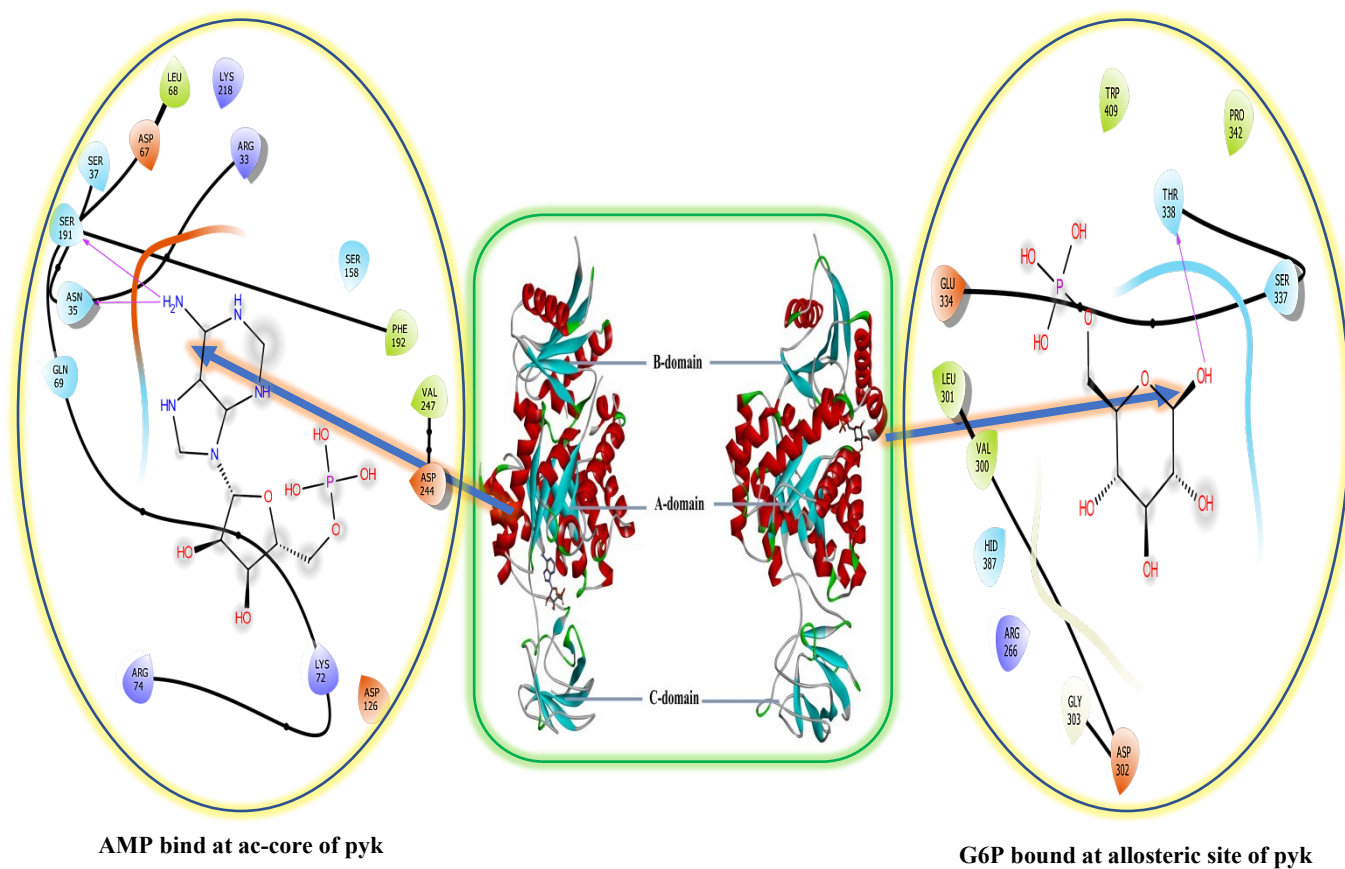


Figure 1: The allosteric site of *M. tuberculosis* Pyk indicating the binding modes of AMP and G6P. The binding mode of effector molecules and interacting residues are indicated in a circular image.

Table 1: Prominent binding site and their residues identification of pyruvate kinase protein model by MetaPocket 2.0 server and reported binding site residues.

Protein name	Predicted prominent binding site residues					Reported binding site residues
Pyruvate Kinase (PyK)	Binding site: 1					
	LEU11	GLY12	PRO13	GLN16	ALA47	Lys72, Arg74, Asn35,
	MET34	HIS44	ASP43	GLY39	HIS38	Leu68, Asp67, Ser37,
	SER314	ASN35	THR10	VAL315	ARG33	Arg266, Leu301,
	SER310	GLY311	THR276	MET308	ASP244	Thr338,
	ASP67	LYS218	GLU220	GLN277	ASP280	Ser337, Trp409,
	ALA241	MET239	SER37	PHE192	SER191	Phe192,
	ALA275	LEU68	GLN69	GLY243	ARG74	Asp126, Val247,
	ILE283	GLU312	MET278	ASP126	VAL247	Asp244,
	LYS72	PRO71	GLY156	SER158	GLY70	Gly303, His387,
	ASP125	LYS155	GLU248	LYS221	ARG242	Val300,
	GLY246	ASN154	ILE157	LEU251	SER170	Glu334, Pro342
	GLU171	LYS172	ILE73	ARG194	VAL164	
	LEU159	VAL254	ALA166	PRO160	MET162	
	PRO255	GLN258	ASP295	LYS259	ASP302	
	ASN298	LEU256	TYR109	LEU112	ILE93	
	VAL95	THR107	ASP139	VAL141	ALA113	
	LYS110	ASP140	ALA116	VAL122	LEU131	
	ASP115	ASP120	ARG111	ASN163	ASP173	
	THR165	ASP40	VAL46	ALA14	LEU169	
	THR108	PRO167	ALA168	GLY127	PRO222	
	Binding site: 2					
	MET239	ILE273				
	Binding site: 3					
	ARG211	ARG212	ASP236	ARG381	VAL213	
	PRO214	MET187	PRO271	GLN404	MET407	
	ILE216	ALA237	PHE373	THR374	GLN375	
	THR396	ALA397	VAL416	TRP398	VAL401	
	GLU400	LYS418	SER376	VAL272	ILE273	
	ASP305	ALA306	VAL456	HIS203	MET206	
	VAL215	ASP207	ALA234	VAL199	PHE235	
	ASP378	GLY454	THR455	PRO453	GLY377	
	LYS270	ALA269	ARG382	ARG351	THR379	
	ASN268	ARG385	VAL232	LEU233	GLU267	
	GLU229	ALA230	MET264	THR349	PRO347	
	ARG266	GLY352	ILE346	LEU386	SER355	
	TYR356	ARG348	VAL353	LYS350	HIS345	
	LEU343					

Table 2: Molecular Docking of pyruvate kinase from *M. tuberculosis* with AMP and G6P

Ligand	Binding Energy (Kcal/mol)	Protein-Ligand Interaction			
		Number of H-bonds	Residues involved in H-bond interactions	Distance between residues and ligand molecule (Å)	Hydrophobic Interactions
Adenosine monophosphate (AMP)	-7.4	6	Lys 72	2.98	Phe 192
			Arg 74	2.96; 3.06	Asp 126
			Asn 35	3.27	Val 247
			Leu 68	2.96	Asp 244
			Asp 67	3.01	
			Ser 37	3.01	
Glucose-6-phosphate (G6P)	-6.3	5	Arg 266	3.09; 3.18	Gly 303
			Leu 301	3.04	His 387
			Thr 338	3.01; 3.04	Val 300
			Ser 337	2.97; 2.96	Glu 334
			Trp 409	2.93	Pro 342

Conformational Flexibility and Stability Analysis

All the backbone atoms relative to the three trajectories for pyk, pyk-AMP and pyk-G6P models were analysed with respect to root-mean-square deviations (RMSD) to determine the system equilibrium. It is frequently observed that the stability of the system was indicated by small RMSD values and additionally the experimental structures were constructed by newly constructed models. However, large conformational changes are justified by higher RMSD values [39]. The pairwise distance distribution (distance RMSD) was used to analyse the structural and dynamic differences in the native and ligand-bound pyk structure from the *M. tuberculosis*. During the simulation, the interaction distance is calculated at each time factor and the frequency distribution of the distance between a pair of residues as plotted in Figure 2A.

The RMSF of the backbone atoms of each residue in the pyk, pyk-AMP and pyk-G6P complex was analysed to check the flexibility of the enzyme backbone structure. The RMSF graph for unbound and bound complexes of pyruvate kinase with G6P and AMP is shown in Figure 2B. pyk-AMP complex attained a high level of fluctuation in the residue positions 90-100. The residues 280-300 have shown great fluctuation from 0.35- 0.4 nm and the fluctuations at certain residues are seen to be very high and large. In contrast, the residues 70-100 of pyk-G6P complex had shown maximum fluctuation. Further information on RMSD and RMSF is provided in SI 5 and SI 6.

Intermolecular Hydrogen Bonds Stabilize the Enzyme Complex

The stabilization of the protein-ligand complex is achieved by the formation of intermolecular H-bonds between the protein and ligand. The stability of the hydrogen bond

network formed between G6P and AMP is calculated throughout 10 ns simulation period. The total number of H-bonds in the pyk-G6P and pyk-AMP versus time at 300K is shown in Figure 2C. Pyk-G6P complex exhibited continuous formation of H-bonds throughout the simulation period, indicating G6P binding is stabilizing the pyk (Figure 2C).

Analysis of Correlation and Minimum-Distance Matrices

The particular residue fluctuations can be analysed by B-factors. No notable information is provided by the B-factor analyses about the correlation between fluctuations of two different residues. The ΔR_i and ΔR_j of i^{th} and j^{th} α -carbon is the measure of their fluctuations which can be assessed by calculating the projection of one on another, i.e., $\langle \Delta R_i \cdot \Delta R_j \rangle$ at every instant and averaging over the full trajectory. The positive correlation of $\langle \Delta R_i \cdot \Delta R_j \rangle$ indicates that the two residues move, on average in the same direction. The positive correlation indicates the movement of two residues on average in the same direction, while, a negative correlation shows the movement of two atoms in the opposite direction. The displacement of two residues equally in the same direction suggests that their motions are positively correlated [40]. The correlation plots obtained show (Figure 3A) that the magnitude of anticorrelated movements of the active site of an enzyme (cleft between A and B domain) is reduced upon the binding of G6P and AMP, which support that G6P decreases molecular motions leading to the formation of stable conformation. These correlated motions of the pyruvate kinase show that G6P binding keeps the enzyme in active R-state conformation. The transition from 'T' to 'R' state of Mtb-pyk suggests that the substrate PEP binds to a distinct active site other than the short α -helix effector binding site adopting an ordered conformation.

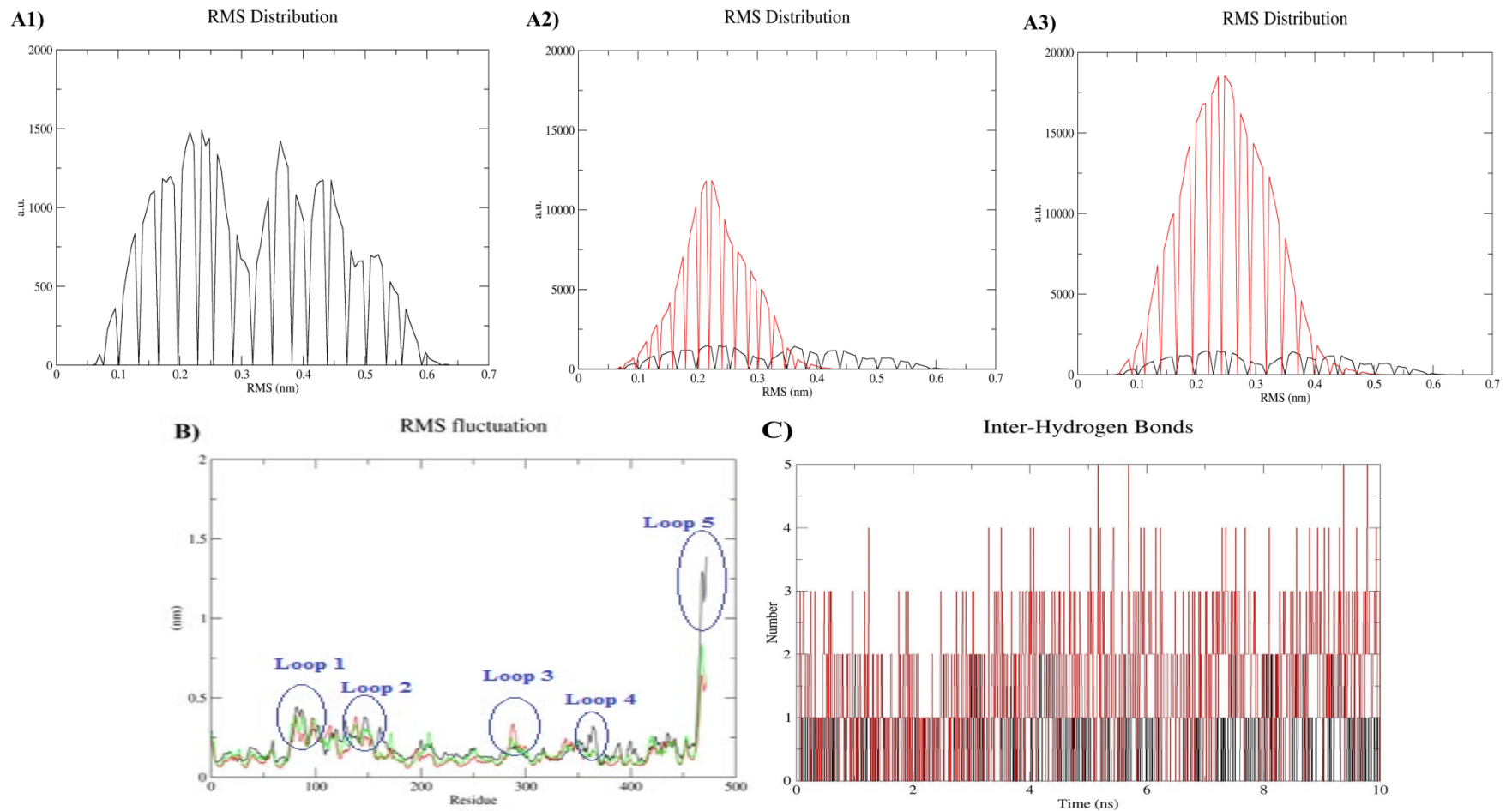


Figure 2: Analysis of MD simulations of the pyk, pyk-AMP and pyk-G6P complex to study the stability and conformational flexibility of enzyme. The plots illustrate the distribution of the distances between the residues for the (A1) pyk (apo state), (A2) pyk-AMP and (A3) pyk-G6P (holo state) obtained for MD simulation. (B) Comparison of root means square fluctuations (RMSFs) of the $C\alpha$ atoms of the *M. tuberculosis* pyk monomer apo structure (Black color) with the holo-structure pyk-AMP (Red color) and pyk-G6P (Green color) calculated from MD simulation showing the enhanced mobility of the B-domain residues (Loop 1, Loop 2 and Loop 5) when compared to A and C domains (Loop 3 and Loop 4) as indicated in the Figure. (C) Inter-molecular Hydrogen-bonding analysis, for the period of simulation time under consideration the formation of hydrogen bonds for stabilizing the structure of Pyk-AMP (Black) and Pyk-G6P (Red).

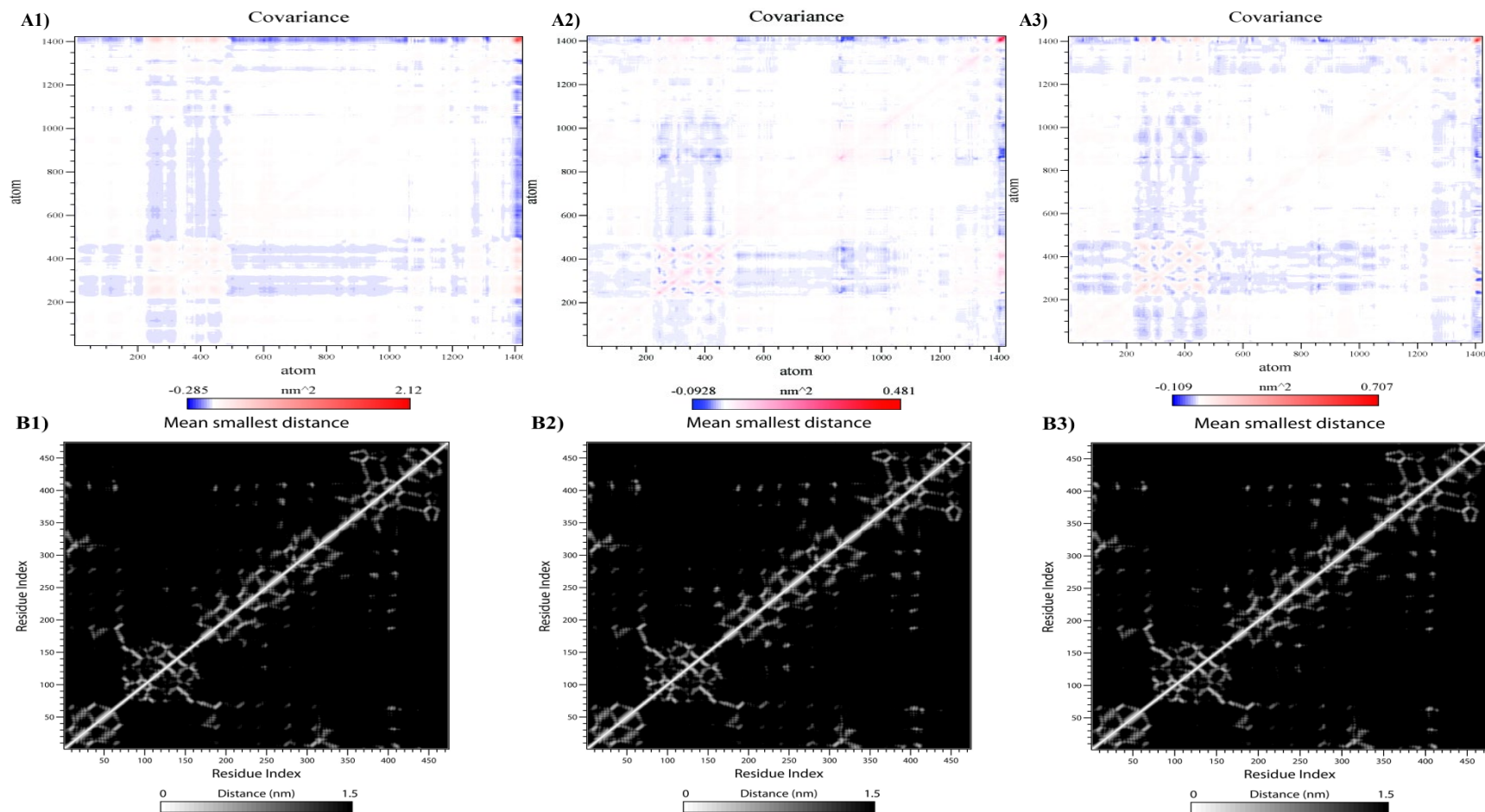


Figure 3: (A1-A3) Covariance matrix of PCA for MD simulation over 10 ns. Red means that two atoms move together, so it is reasonable that on diagonal there is a red line. Blue means that they move in opposite directions. The intensity of colors indicates the amplitude of the fluctuations. From the covariance matrix, it is possible to see that group of atoms move in a correlated or anti-correlated manner. (B1-B3) The average of the minimum smallest distance matrix between the pair of atoms at a time scale of 10ns MD simulation for pyruvate kinase. A plot of the distance between two atoms or the minimum distance between two groups or atoms provides information about contacts in the protein. The plots showing the distances between all residues of the protein furnish a symmetrical matrix. Plotting these matrices for different time frames, one can analyse changes in the structure upon effector molecule binding.

The shaded regions shown in Figure 3B1 suggest that the *pyk* is strongly anticorrelated than those of the holo-structures of *pyk* bound with ligands. This shows that the ligand binding decreases the negative correlation of the mobile B-domain and its binding region (C-domain). The ligand G6P sits in the effector binding pocket by interaction with Leu301, Arg266, Thr338, Ser337 and Trp409. The distance between these residues with G6P bound is 3.04 Å, 3.18 Å, 3.04 Å, 2.97 Å and 2.93 Å, respectively (Figure 3B3). The motions of the AC-cores in *pyk* require the disruption of C-C interface interactions between the AMP loop (Figure 3B2) and the C-terminal tail loop as well as the hydrogen bonds formed between the two adjacent Cα4 structures.

The distance between all residues of the protein was obtained by symmetrical matrix analysis. By plotting these matrices for different time frames on protein complexes of the simulation, changes in the conformation of a protein can be obtained. In our analysis, a total of 10 matrices for 472 residues for every 1000ps were plotted to study the changes in the structure (SI 7). Minimum distance between two residues is the smallest distance between any pair of atoms showing changes in the structure. Plotting these matrices for different time frames, one can analyse changes in the structure. During the entire simulation, there is a large ratio increase in the number of contacts between the residues with nearly 1250 ratios. As Figure 3B shows the time scale of all the simulations, there is a minimum distance between the residues of the protein groups at nearly 7800 ps with 0.0999.

Global Motions in Pyruvate Kinase

The theoretical and experimental B-factors are compared using two corresponding 2D interactive graphs that provide experimental data on the spatial fluctuations of atoms in a crystal environment (SI 8.1). The movement of the structural elements together in the particular mode is given by measuring the degree of collectivity of a given mode. The high degree collectivity of a mode related to functional importance, which seems to be found at the low-frequency end of the spectrum (SI 8.2). Higher values of frequency distribution indicate a low-frequency slowest mode, which is high relative to the biological function (SI 8.3).

Functional Site Analysis Based on Dynamics

The functional site and signal communication of *pyk*-G6P and *pyk*-AMP was predicted by using elastic network model (EMN) 1.0. Computing the monomeric pyruvate kinase in

complex with AMP and G6P using the COMPACT algorithm with two slowest Gaussian network model (GNM) modes show that the allosteric site which is predicted with high sensitivity and moderate specificity (Figure 4). The residues Val238, Asp305, Met407, Lys270, Leu190, Lys6, Arg242, Leu228, and Asn35 are predicted as potential functional sites (PFSs) in the given structure complex.

All PFSs including allosteric sites were verified to be conserved in support of their functional significance. The signalling/communication sites obtained for pyruvate kinase in complex with AMP and G6P were shown in Figure 5. The left panel displays the hitting times [41], H_{ij} organized in a 2D map, color-coded from red to blue, in the order of increasing hitting time.

The graph-theoretical concepts such as hitting and communication times are based on the Markovian processing of the signal across the network. The propensity of residues to send signals (left-color coded) or to receive signals (right-color coded) has been shown in Figure 5A and 5B. The higher propensity for allosteric communication was achieved with small hitting times (as a receiver or broadcaster) with the values for individual residues deduced from the 2D maps (Figure 5C) by taking the average of rows and columns in the matrix as indicated.

The signalling rate is direction-dependent, illustrating the matrix as asymmetric. The profile on the right hand (average column vector) side shows the predisposition of particular residues to receive signals. A minimal hitting (average of overall signal communicating sites) was exhibited by catalytic residues as found in earlier observations shown in Figure 5. The strength of the response by residue i to the perturbation at residue j was described by color code map [42]. The residues highly sensitive to perturbations were indicated by peaks with average profile and could serve as effectors or sensors, respectively.

The sensor and effector residues were also predicted as illustrated in Figure 6, where residues with high sensor or effector are shown in dark red color. The lowest frequency mode 1 of the pyruvate kinase complex was sampled based on the RMSD of 4 Å with respect to the 3D structure. The PRS map as illustrated in Figure 6, dark red color shows strong responses and the peaks along the curve indicate the residues that can potentially serve as sensors and effectors. Cross-correlations between residue motions in the presence of AMP and G6P, based on 20 softest modes are illustrated in the map. The peak along the curve indicates that the residues can potentially serve as sensors (below the map) and effectors (right side of the map). (SI 8.4 – SI 8.8).

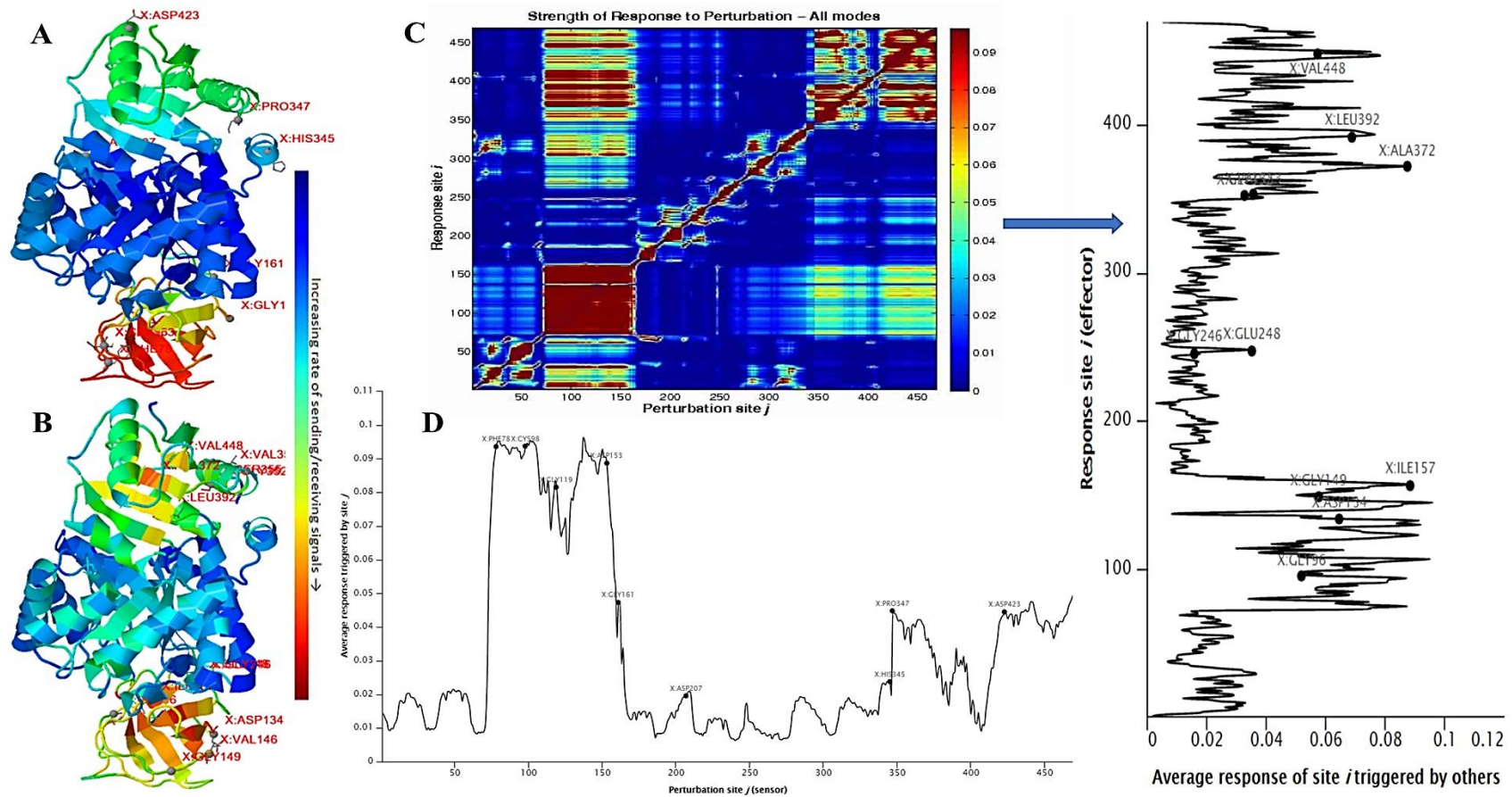


Figure 6: Effect of allosteric effectors (AMP and G6P) on the structural dynamics of pyruvate kinase. **(A-B)** Indicate the sensor and effector residues respectively. The colour code from blue to red indicates the increase in the propensity of residues to act as sensors or effectors. The strongest responses (sensors/ effectors) are shown in dark red color in the PRS map **(C)** and the peaks indicate the residues possessing effector property (right side of the map in **C**). The peaks along the curve indicate the residues that potentially serve as sensors **(D)**.

DISCUSSION

During glycolysis, the phosphoenolpyruvate and adenosine diphosphate (ADP) are transformed into pyruvate and adenosine triphosphate (ATP), catalysed by a homotetrameric pyk as a final step of glycolysis. Further, the pyruvate harbours into numerous metabolic pathways during which pyruvate kinase acts as a hub protein and is perceived to be a prime factor in regulating glycolytic energy generation [43–47]. During the non-replicative state within the host, *M. tuberculosis* relies on fatty acid metabolism [16], despite glycolysis playing a major role under certain circumstances *in-vivo*, as *M. tuberculosis* maintains a functional intact flux throughout as a rate-limiting step in the glycolytic pathway [48]. *In-vivo* studies in mice have ensured that gluconeogenesis is indispensable for the survival of *M. tuberculosis*, which indicates that the glycolytic substrate cannot be extracted from the host [3]. *Mycobacterium bovis* containing an inactive pyruvate kinase, corroborate this theory by demonstrating the inability of the organism to metabolize fermentable carbon source [49]. Fundamentally, pyruvate kinase facilitates glycolytic and gluconeogenic substrates imperative for the detoxification of sugar phosphates during glucose metabolism besides fatty acid metabolism.

In-vitro evidence has shown multiple co-catabolism of carbon sources all at once rather than the preference of carbon catabolite repression (CCR) seen in *M. tuberculosis* [50]. The experimental evidence from *M. tuberculosis* suggests that the allosteric mechanism in pyruvate kinase is regulated neither by fructose 1, 6-bisphosphate (FBP) nor by ribose 5-phosphate (R5P), but by regulators such as glucose-6-phosphate and AMP which show a prominent function in carbon catabolic control through feed-forward fashion [6].

In the present work, high stability was observed in the 'T'-state of the enzyme (unbound) based on the RMSD values of pyk. The protein in each conformation consists of three domains such as A, B and C, i.e., A-domain forms a classic (α/β)₈ topology, the B-domain with a moderately irregular fold (mobile lid) and C-domain with the alpha/beta organization [42]. The structural transitions in the A-domain and C-domain interface result in proximity and relative rotation of two domains in the stable state, which is confirmed by the variations observed in the RMSF plot (Figure 2), suggesting large variations associated with enzyme conformation in the ligand-bound holoenzyme. This results in the transition of T-state (inactive) to R-state (active), which comprises a rigid body rotation of 9° [51] at the AC-core (A and C domain) assumed as a pivotal point. Both the rigid domain movements and local flexibility are found to be essentially required during allosteric regulation of *M. tuberculosis* pyk notably during stress conditions (host infection) to maintain the high level of carbon metabolism. In this context, the shift between the T-state and R-state of the enzyme is associated with the symmetrically vibrational motions of the A and C-domain cores, which control the

regulatory switch [18]. The enzyme (pyk) in R-state is stabilized by binding of substrate, whereas G6P (effector) binding activates enzyme activity. Further, the molecular motions of the pyk with and without G6P bound have shown that the structure of pyk was found to be fluctuating slightly more when compared to G6P bound pyk enzyme (Figure 1). The RMSF for pyk alone over the time period of simulation indicates relative instability and disorder of the α -helix (C-domain), in comparison to the holoenzyme (pyk bound with effectors G6P and AMP), which appears to be stable and ordered (active R-state) during the period of simulation.

CONCLUSION

It is quite interesting to note that the change of correlation upon binding of the effector molecule decreases the motions of A-domain's acidic residues. The matrices obtained are consistent with the interpretation of the temperature factor analysis, which forms the weakened anticorrelated movements between the B-domain and A-domain residues and between the C-domain residues. The interplay between the AMP loop and the C-terminal chain loop favor the formation of R-conformation during the transition between T-and R-states. The G6P binding site in *M. tuberculosis* pyk reveals the allosteric site is located distinctly from the AMP-binding allosteric site, which is situated between the A and C domains composed of helix A α 6, Ca1, Ca2 and G6P-loop. The synergistic assistance of two allosteric binding sites for AMP and G6P in *M. tuberculosis* pyk monomer provides evidence for the existence of two physical allosteric pathways in the bacterium to regulate several metabolic processes.

ACKNOWLEDGMENT

The authors are thankful to Registrar, Nitte (Deemed to be University), Mangalore, India, for providing all the facilities to complete this work.

CONFLICT OF INTEREST

The authors declare that there is no conflict of interest regarding the publication of this manuscript.

REFERENCES

1. WHO. Global Tuberculosis Report 2016, World Health Organization. [Http://Apps.Who.Int/Iris/Bitstream/10665/91355/1/9789241564656_Eng.Pdf](http://apps.who.int/iris/bitstream/10665/91355/1/9789241564656_Eng.Pdf). 2016, pp 2014–2016.
2. Bai, N. J., Pai, M. R., Murthy, P. S., Venkatasubramanian, T. A. (1975) Pathways of Carbohydrate Metabolism in *Mycobacterium Tuberculosis* H37Rv. *Can. J. Microbiol.* 21 (11), 1688–1691. <https://doi.org/10.1139/m75-247>.
3. Marrero, J., Rhee, K. Y., Schnappinger, D., Pethe, K., Ehrh, S. (2010) Gluconeogenic Carbon Flow of Tricarboxylic Acid Cycle Intermediates Is Critical for *Mycobacterium Tuberculosis* to Establish

- and Maintain Infection. *Proc. Natl. Acad. Sci. U. S. A.* 107 (21), 9819–9824. <https://doi.org/10.1073/pnas.1000715107>.
4. Nandakumar, M., Nathan, C., Rhee, K. Y. (2014) Isocitrate Lyase Mediates Broad Antibiotic Tolerance in Mycobacterium Tuberculosis. *Nat. Commun.* 5. <https://doi.org/10.1038/ncomms5306>.
 5. Trujillo, C., Blumenthal, A., Marrero, J., Rhee, K. Y., Schnappinger, D., Ehrt, S. (2014) Triosephosphate Isomerase Is Dispensable in Vitro yet Essential for Mycobacterium Tuberculosis to Establish Infection. *MBio* 5 (2). <https://doi.org/10.1128/mBio.00085-14>.
 6. De Carvalho, L. P. S., Fischer, S. M., Marrero, J., Nathan, C., Ehrt, S., Rhee, K. Y. (2010) Metabolomics of Mycobacterium Tuberculosis Reveals Compartmentalized Co-Catabolism of Carbon Substrates. *Chem. Biol.* 17 (10), 1122–1131. <https://doi.org/10.1016/j.chembiol.2010.08.009>.
 7. Somashekar, B. S., Amin, A. G., Rithner, C. D., Troudt, J., Basaraba, R., Izzo, A., Crick, D. C., Chatterjee, D. (2011) Metabolic Profiling of Lung Granuloma in Mycobacterium Tuberculosis Infected Guinea Pigs: Ex Vivo 1 H Magic Angle Spinning NMR Studies. *J. Proteome Res.* 10 (9), 4186–4195. <https://doi.org/10.1021/pr2003352>.
 8. Noy, T., Vergnolle, O., Hartman, T. E., Rhee, K. Y., Jacobs, W. R., Berney, M., Blanchard, J. S. (2016) Central Role of Pyruvate Kinase in Carbon Co-Catabolism of Mycobacterium Tuberculosis. *J. Biol. Chem.* 291 (13), 7060–7069. <https://doi.org/10.1074/jbc.M115.707430>.
 9. Martínez Cuesta, S., Rahman, S. A., Furnham, N., Thornton, J. M. (2015) The Classification and Evolution of Enzyme Function. *Biophysical Journal.* 1082–1086. <https://doi.org/10.1016/j.bpj.2015.04.020>.
 10. Meehan, C. J., Goig, G. A., Kohl, T. A., Verboven, L., Dippenaar, A., Ezewudo, M., Farhat, M. R., Guthrie, J. L., Laukens, K., Miotto, P., et al. (2019) Whole Genome Sequencing of Mycobacterium Tuberculosis: Current Standards and Open Issues. *Nat. Rev. Microbiol.* 17 (9), 533–545. <https://doi.org/10.1038/s41579-019-0214-5>.
 11. Tulloch, L. B., Morgan, H. P., Hannaert, V., Michels, P. A. M., Fothergill-Gilmore, L. A., Walkinshaw, M. D. (2008) Sulphate Removal Induces a Major Conformational Change in Leishmania Mexicana Pyruvate Kinase in the Crystalline State. *J. Mol. Biol.* 383 (3), 615–626. <https://doi.org/10.1016/j.jmb.2008.08.037>.
 12. Jurica, M. S., Mesecar, A., Heath, P. J., Shi, W., Nowak, T., Stoddard, B. L. (1998) The Allosteric Regulation of Pyruvate Kinase by Fructose-1,6-Bisphosphate. *Structure* 6 (2), 195–210. [https://doi.org/10.1016/S0969-2126\(98\)00021-5](https://doi.org/10.1016/S0969-2126(98)00021-5).
 13. Larsen, T. M., Laughlin, L. T., Holden, H. M., Rayment, I., Reed, G. H. (1998) Structure of Rabbit Muscle Pyruvate Kinase Complexed with Mn²⁺, K⁺, and Pyruvate. *Biochemistry* 33 (20), 6301–6309. <https://doi.org/10.1021/bi00186a033>.
 14. Morgan, H. P., McNae, I. W., Nowicki, M. W., Hannaert, V., Michels, P. A. M., Fothergill-Gilmore, L. A., Walkinshaw, M. D. (2010) Allosteric Mechanism of Pyruvate Kinase from Leishmania Mexicana Uses a Rock and Lock Model. *J. Biol. Chem.* 285 (17), 12892–12898. <https://doi.org/10.1074/jbc.M109.079905>.
 15. Zoraghi, R., See, R. H., Axerio-Cilies, P., Kumar, N. S., Gong, H., Moreau, A., Hsing, M., Kaur, S., Swayze, R. D., Worrall, L., et al. (2011) Identification of Pyruvate Kinase in Methicillin-Resistant Staphylococcus Aureus as a Novel Antimicrobial Drug Target. *Antimicrob. Agents Chemother.* 55 (5), 2042–2053. <https://doi.org/10.1128/AAC.01250-10>.
 16. Enriqueta Muñoz, M., Ponce, E. (2003) Pyruvate Kinase: Current Status of Regulatory and Functional Properties. *Comparative Biochemistry and Physiology - B Biochemistry and Molecular Biology.* 197–218. [https://doi.org/10.1016/S1096-4959\(03\)00081-2](https://doi.org/10.1016/S1096-4959(03)00081-2).
 17. Lindsley, J. E., Rutter, J. (2006) Whence Cometh the Allosterome? *Proc. Natl. Acad. Sci.* 103 (28), 10533–10535. <https://doi.org/10.1073/pnas.0604452103>.
 18. Zhong W, Cui L, Goh BC, Cai Q, Ho P, Chionh YH, Yuan M, Sahili AE, Fothergill-Gilmore LA, Walkinshaw MD, Lescar J, Dedon PC. Allosteric pyruvate kinase-based "logic gate" synergistically senses energy and sugar levels in Mycobacterium tuberculosis. *Nat Commun.* 2017 Dec 7;8(1):1986. doi: 10.1038/s41467-017-02086-y.
 19. Ahmad, S., Ali, M. M., Mustafa, A. S. (2003) Construction of a Modified Vector for Efficient Purification of Recombinant Mycobacterium Tuberculosis Proteins Expressed in Escherichia Coli. *Protein Expr. Purif.* 29 (2), 167–175. [https://doi.org/10.1016/S1046-5928\(03\)00052-4](https://doi.org/10.1016/S1046-5928(03)00052-4).
 20. Webb, B., Sali, A. (2016) Comparative Protein Structure Modeling Using MODELLER. *Curr. Protoc. Bioinforma.* 2016, 5.6.1-5.6.37. <https://doi.org/10.1002/cpbi.3>.
 21. Gollapalli P., Hanumanthappa, M. (2016) Conformational Flexibility and Dynamic Properties in Allosteric Regulation of Mycobacterium Tuberculosis Pyruvate Kinase. *MOJ Proteomics Bioinforma.* 4 (3). <https://doi.org/10.15406/mojpb.2016.04.00128>.
 22. Kim, S., Thiessen, P. A., Bolton, E. E., Chen, J., Fu, G., Gindulyte, A., Han, L., He, J., He, S., Shoemaker, B. A., et al. (2016) PubChem Substance and Compound Databases. *Nucleic Acids Res.* 44 (D1), D1202–D1213. <https://doi.org/10.1093/nar/gkv951>.
 23. Raghavendra, S., Aditya Rao, S. J., Kumar, V., Ramesh, C. K. (2015) Multiple Ligand Simultaneous Docking (MLSD): A Novel Approach to Study the Effect of Inhibitors on Substrate Binding to PPO. *Comput. Biol. Chem.* 59, 81–86. <https://doi.org/10.1016/j.compbiolchem.2015.09.008>.
 24. Huang, B. (2009) Metapocket: A Meta Approach to Improve Protein Ligand Binding Site Prediction. *Omi. A J. Integr. Biol.* 13 (4), 325–330. <https://doi.org/10.1089/omi.2009.0045>.
 25. Schneidman-Duhovny, D., Inbar, Y., Nussinov, R., Wolfson, H. J. (2005) PatchDock and SymmDock: Servers for Rigid and Symmetric Docking. *Nucleic Acids Res.* 33 (SUPPL. 2). <https://doi.org/10.1093/nar/gki481>.
 26. Trott, O., Olson, A. J. (2010) Software News and Update AutoDock Vina: Improving the Speed and Accuracy of Docking with a New Scoring Function, Efficient Optimization, and Multithreading. *J. Comput. Chem.* 31 (2), 455–461. <https://doi.org/10.1002/jcc.21334>.
 27. Aditya Rao, S. J., Ramesh, C. K., Raghavendra, S., Paramesha, M. (2019) Dehydroabietylamine, a Diterpene from Carthamus Tinctorius L. Showing Antibacterial and Anthelmintic Effects with Computational Evidence. *Curr. Comput. Aided. Drug Des.* 15. <https://doi.org/10.2174/1573409915666190301142811>.
 28. Janakirama, A.R.S., Shivayogi, S.M., Satyanarayana, J.K., Kumaran, R.C., (2020) Characterization of isolated compounds from Morus spp. and their biological activity as anticancer molecules. *BioImpacts.* 11. <https://doi.org/10.34172/bi.2021.09>.
 29. Fitzgerald, C.E., Patel, S.B., Becker, J.W., Cameron, P.M., Zaller, D., Pikounis, V.B., O’Keefe, S.J., Scapin, G., (2003) Structural basis for p38 α MAP kinase quinazolinone and pyridol-pyrimidine inhibitor specificity. *Nat. Struct. Biol.* 10, 764–769. <https://doi.org/10.1038/nsb949>.
 30. Aditya R, Venugopal T, Jayanna N, Paramesha M, Ramesh C. (2020) Bioactive isolates of Morus species as antibacterial agents and their insilico profiling. *Lett Drug Des Discov.* 17. <https://doi.org/10.2174/1570180817999201104120815>

31. Lindahl, E., Hess, B., Kutzner, C., van der Spoel, D. (2008) Gromacs 4.0: Algorithms for Highly Efficient, Load-Balanced, and Scalable Molecular Simulation. *J. Chem. Theory Comput.* 4, 435–447.
32. Berendsen, H. J. C., Postma, J. P. M., Van Gunsteren, W. F., Dinola, A., Haak, J. R. (1984) Molecular Dynamics with Coupling to an External Bath. *J. Chem. Phys.* 81 (8), 3684–3690. <https://doi.org/10.1063/1.448118>.
33. Ryckaert, J. P., Ciccotti, G., Berendsen, H. J. C. (1977) Numerical Integration of the Cartesian Equations of Motion of a System with Constraints: Molecular Dynamics of N-Alkanes. *J. Comput. Phys.* 23 (3), 327–341. [https://doi.org/10.1016/0021-9991\(77\)90098-5](https://doi.org/10.1016/0021-9991(77)90098-5).
34. Tara, S., Straatsma, T. P., McCammon, J. A. (1999) Mouse Acetylcholinesterase Unliganded and in Complex with Huperzine A: A Comparison of Molecular Dynamics Simulations. *Biopolymers* 50 (1), 35–43. [https://doi.org/10.1002/\(SICI\)1097-0282\(199907\)50:1<35::AID-BIP4>3.0.CO;2-6](https://doi.org/10.1002/(SICI)1097-0282(199907)50:1<35::AID-BIP4>3.0.CO;2-6).
35. Jolliffe, I. T. T. (2002) *Principal Component Analysis*, Second Edition, New York: Springer Science & Business Media.
36. Amadei, A., Chillemi, G., Ceruso, M. A., Grottesi, A., Di Nola, A. (2000) Molecular Dynamics Simulations with Constrained Roto-Translational Motions: Theoretical Basis and Statistical Mechanical Consistency. *J. Chem. Phys.* 112 (1), 9–23. <https://doi.org/10.1063/1.480557>.
37. Hughes, G. F. (1968) On the Mean Accuracy of Statistical Pattern Recognizers. *IEEE Trans. Inf. Theory* 14 (1), 55–63. <https://doi.org/10.1109/TIT.1968.1054102>.
38. Li, H., Chang, Y. Y., Lee, J. Y., Bahar, I., Yang, L. W. (2017) DynOmics: Dynamics of Structural Proteome and beyond. *Nucleic Acids Res.* 45 (W1), W374–W380. <https://doi.org/10.1093/nar/gkx385>.
39. Meng, H., Li, C., Wang, Y., Chen, G. (2014) Molecular Dynamics Simulation of the Allosteric Regulation of eIF4A Protein from the Open to Closed State, Induced by ATP and RNA Substrates. *PLoS One* 9 (1). <https://doi.org/10.1371/journal.pone.0086104>.
40. Naithani, A., Taylor, P., Erman, B., Walkinshaw, M. D. (2015) A Molecular Dynamics Study of Allosteric Transitions in *Leishmania Mexicana* Pyruvate Kinase. *Biophys. J.* 109 (6), 1149–1156. <https://doi.org/10.1016/j.bpj.2015.05.040>.
41. Chennubhotla, C., Bahar, I. (2007) Signal Propagation in Proteins and Relation to Equilibrium Fluctuations. *PLoS Comput. Biol.* 3 (9), 1716–1726. <https://doi.org/10.1371/journal.pcbi.0030172>.
42. (39) Mattevi, A., Valentini, G., Rizzi, M., Speranza, M. L., Bolognesi, M., Coda, A. (1995) Crystal Structure of *Escherichia Coli* Pyruvate Kinase Type I: Molecular Basis of the Allosteric Transition. *Structure* 3 (7), 729–741. [https://doi.org/10.1016/S0969-2126\(01\)00207-6](https://doi.org/10.1016/S0969-2126(01)00207-6).
43. Zoraghi, R., See, R. H., Gong, H., Lian, T., Swayze, R., Finlay, B. B., Brunham, R. C., McMaster, W. R., Reiner, N. E. (2010) Functional Analysis, Overexpression, and Kinetic Characterization of Pyruvate Kinase from Methicillin-Resistant *Staphylococcus Aureus*. *Biochemistry* 49 (35), 7733–7747. <https://doi.org/10.1021/bi100780t>.
44. Emmerling, M., Bailey, J. E., Sauer, U. (1999) Glucose Catabolism of *Escherichia Coli* Strains with Increased Activity and Altered Regulation of Key Glycolytic Enzymes. *Metab. Eng.* 1 (2), 117–127. <https://doi.org/10.1006/mben.1998.0109>.
45. Fry, B., Zhu, T., Domach, M. M., Koepsel, R. R., Phalakornkule, C., Ataai, M. M. (2000) Characterization of Growth and Acid Formation in a *Bacillus Subtilis* Pyruvate Kinase Mutant. *Appl. Environ. Microbiol.* 66 (9), 4045–4049. <https://doi.org/10.1128/AEM.66.9.4045-4049.2000>.
46. Ramos, A., Neves, A. R., Ventura, R., Maycock, C., López, P., Santos, H. (2004) Effect of Pyruvate Kinase Overproduction on Glucose Metabolism of *Lactococcus Lactis*. *Microbiology* 150 (4), 1103–1111. <https://doi.org/10.1099/mic.0.26695-0>.
47. Al Zaid Siddiquee, K., Arauzo-Bravo, M. J., Shimizu, K. (2004) Metabolic Flux Analysis of pykF Gene Knockout *Escherichia Coli* Based on ¹³C-Labeling Experiments Together with Measurements of Enzyme Activities and Intracellular Metabolite Concentrations. *Appl. Microbiol. Biotechnol.* 63 (4), 407–417. <https://doi.org/10.1007/s00253-003-1357-9>.
48. Kayne, F. J. Pyruvate Kinase. (1973) In *Group Transfer Part A: Nucleotidyl Transfer Nucleosidyl Transfer Acyl Transfer Phosphoryl Transfer*; Boyer, P. D., Ed.; The Enzymes; Academic Press, Vol. 8, pp 353–382. [https://doi.org/https://doi.org/10.1016/S1874-6047\(08\)60071-2](https://doi.org/https://doi.org/10.1016/S1874-6047(08)60071-2).
49. Chavadi, S., Wooff, E., Coldham, N. G., Sritharan, M., Hewinson, R. G., Gordon, S. V., Wheeler, P. R. (2009) Global Effects of Inactivation of the Pyruvate Kinase Gene in the *Mycobacterium Tuberculosis* Complex. *J. Bacteriol.* 191 (24), 7545–7553. <https://doi.org/10.1128/JB.00619-09>.
50. Kovárová-Kovar, K., Egli, T. (1998) Growth Kinetics of Suspended Microbial Cells: From Single-Substrate-Controlled Growth to Mixed-Substrate Kinetics. *Microbiol. Mol. Biol. Rev.* 62 (3), 646–666.
51. Zhong, W., Cui, L., Goh, B. C., Cai, Q., Ho, P., Chionh, Y. H., Yuan, M., Sahili, A. El, Fothergill-Gilmore, L. A., Walkinshaw, M. D., et al. (2017) Allosteric Pyruvate Kinase-Based “logic Gate” synergistically Senses Energy and Sugar Levels in *Mycobacterium Tuberculosis*. *Nat. Commun.* 8 (1). <https://doi.org/10.1038/s41467-017-02086-y>.